Correlation between Electrolyte Chemistry and Solid Electrolyte Interphase for Reversible Ca Metal Anodes

Zhen Hou[a], Rui Zhou[a], Yunduo Yao[a], Zhiwen Min[b], Ziheng Lu*[c], Ye Zhu[a], Jean-Marie Tarascon[d] and Biao Zhang*[a]

[a] Dr. Z. Hou, R. Zhou, Y. Yao, Prof. Y. Zhu, Prof. B. Zhang
Department of Applied Physics & Research Institute for Smart Energy
The Hong Kong Polytechnic University
Hung Hom, Hong Kong, China
E-mail: biao.ap.zhang@polyu.edu.hk
[b] Z. Min
Shenzhen Institutes of Advanced Technology
Chinese Academy of Sciences
Shenzhen 518055, China
[c] Dr. Z. Lu
Microsoft Research
Beijing 100080, China
E-mail: zihenglu@microsoft.com
[d] Prof. J. M. Tarascon
Chimie du Solide-Energie, UMR 8260
Collège de France
Paris, France

Supporting information for this article is given via a link at the end of the document.

Abstract: The development of rechargeable Ca metal batteries (RCMBs) is hindered by the Ca^{2+} passivating solid electrolyte interphases (SEIs). The cation solvation structure dictated by electrolyte chemistry plays a critical role in the SEIs properties. While a relatively weak cation-solvent binding is preferred in Li metal anodes to promote anion-derived SEIs, we demonstrate an enhanced Ca deposition/stripping reversibility under a strong cation-solvent interaction, which is materialized in strongly-solvating solvent and highly-dissociated salt combinations. Such electrolyte formulations benefit the formation of solvent-occupied solvation structure and minimize the anion reduction, resulting in organic-rich/CaF_2-poor SEIs for reversible Ca metal anodes. Furthermore, RCMBs paired with an organic cathode using the optimized electrolytes are demonstrated as a proof-of-concept. Our work reveals the paradigm shift in SEIs design for Ca metal anodes, opening up new opportunities for emerging RCMBs.

Multivalent-ion batteries (e.g., Mg^{2+} and Ca^{2+}) are considered promising candidates for breaking the energy limitation of current Li-ion batteries (LIBs) owing to the multiple electron transfer per charge carrier.[1] Rechargeable Ca metal batteries (RCMBs) have recently attracted rising attention because of the natural abundance of Ca and low redox potential of Ca/Ca^{2+} that is merely 0.17 V higher than Li/Li^+.[2] However, one longstanding challenge for RCMBs roots in the formation of ionic insulating solid electrolyte interphases (SEIs) on Ca metal anodes, which nearly inhibits reversible Ca deposition/stripping.[3] Massive efforts have been devoted to promoting the charge transfer kinetics across SEIs for building practicable Ca metal anodes, with particular attention dedicated to the electrolyte formulations.[4] Ponrouch et al. realize the first reversible Ca anode at elevated temperature (75-100 °C).[5] Motivated by the successful Mg deposition in magnesium borohydride $Mg(BH_4)_2$-based electrolyte,[6] Bruce's group reports the $Ca(BH_4)_2$/tetrahydrofuran (THF) electrolyte allowing stable Ca deposition/stripping at room temperature.[7] Such an electrolyte leads to the formation of CaH_2 in the SEIs for sufficient Ca^{2+} diffusion, although borohydride salt suffers from low anodic stability. More recently, the dilemma is partly resolved by the introduction of calcium tetrakis(hexafluoroisopropyloxy)borate $Ca[B(hfip)_4]_2$ salt into the glyme solvent, showing high oxidative stability of over 4 V.[8]

The impermeability of SEIs resides largely in inorganic components, such as CaF_2 and $CaCO_3$, which exhibit a substantial Ca^{2+} diffusion energy barrier.[9] The situation differs significantly from the SEIs constructed in the alkali metal (Li/Na/K) anodes, where inorganic components, like fluorine-rich species, are desired because they well support fast charge transfer and benefit the stability.[10] The fundamental divergences necessitate a paradigm shift in SEIs design for emerging RCMBs. However, the several encouraging electrolyte recipes reported until now rely on the unique salt/solvent combinations (Literature summary in Table S1).[9, 11] Their extension to other generalized systems, such as commercially available calcium bis(trifluoromethanesulfonyl)imide $Ca(TFSI)_2$ salt, is not satisfactory. Therefore, it calls for a general principle in Ca electrolyte design for tailoring SEIs characteristics.

The cation solvation structure plays a critical role in determining SEIs features.[4b, 9, 12] The Gutmann donor number (DN) has been identified as a powerful parameter in controlling the solvation structure in the electrolyte.[13] Herein, we systematically explore a number of solvents/salts combinations to correlate with SEIs properties. The spectroscopy analysis and theoretical calculations suggest that electrolytes containing high-DN (strongly-solvating) solvent and low-DN (highly-dissociated) salt lead to solvent-dominated solvation sheaths. This helps suppress the salt anion reduction from producing copious

inorganic species to form organic component-dominated SEIs, benefitting the Ca deposition/stripping kinetics.

We firstly focus on the readily available $Ca(TFSI)_2$ salt and explore nine solvents spanning an extensive range of DN (Figure 1a and Table S2). Ca|Ca symmetric cells are fabricated to probe the reversibility under various electrolytes. Based on the Ca deposition/stripping behavior (Figure 1b and Figure S1), the nine electrolytes could be categorized into two groups. Under group 1 electrolytes, containing ethylene carbonate/propylene carbonate (EC/PC), tetraethylene glycol dimethyl ether (TEGDME), dimethoxyethane (DME) and THF solvents, Ca deposition/stripping overpotentials rapidly increase to 5 V. In sharp contrast, much lower overpotentials (< 2 V) are observed in group 2 electrolytes that are made of another five solvents, i.e., trimethyl phosphate (TMP), triethyl phosphate (TEP), dimethylformamide (DMF), 1-methylimidazole (MeIm) and dimethylacetamide (DMAc). We note the solvents in group 2 have high DN (Figure 1a), potentially leading to strong solvation with cations.[14]

We next search for the underlying reasons for the distinct electrochemical behavior under low-DN and high-DN solvents by adopting EC/PC, MeIm and DMAc electrolytes as the model systems. EC/PC is selected from the low-DN group because it is widely used in Li/Na/K ion batteries, while MeIm and DMAc allow stable cycling with attractively low overpotentials of ~0.75 and ~0.50 V, respectively. Besides, both electrolytes deliver a decent rate capability (Figure 1c). Given the comparable ionic conductivities of the three electrolytes (Figure S2), we conjecture that the significant performance discrepancy originates from the electrode/electrolyte interface disparity. Electrochemical impedance spectroscopy (EIS) is collected to examine the interfacial resistance under the three electrolytes. Indeed, the EC/PC electrolyte cell presents a high interfacial

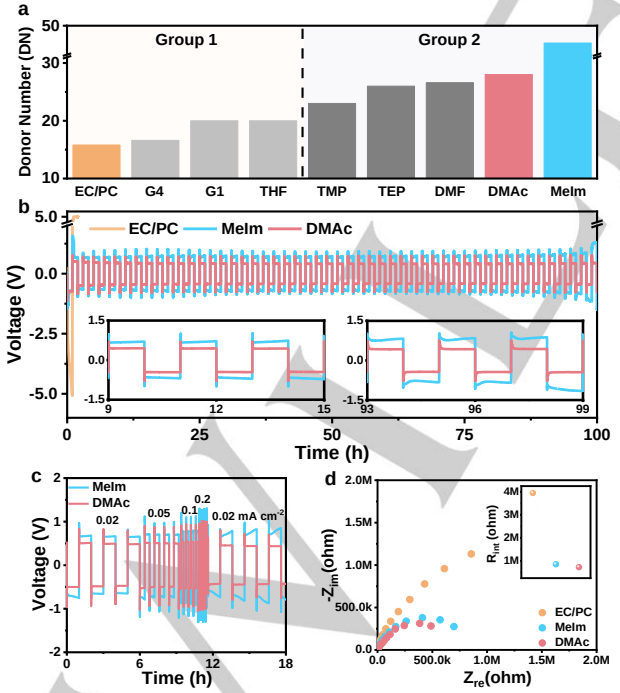

Figure 1. Relationship between Ca reversibility and $Ca(TFSI)_2$-based electrolytes. a) DN of various solvents. b) Cyclic stability at 0.02 mA cm^{-2} and c) rate capability of Ca|Ca symmetric cells in various solvents containing 0.1 M $Ca(TFSI)_2$. d) Nyquist plots of Ca|Ca symmetric cells in various solvents containing 0.1 M $Ca(TFSI)_2$. The inset shows their R_{int}.

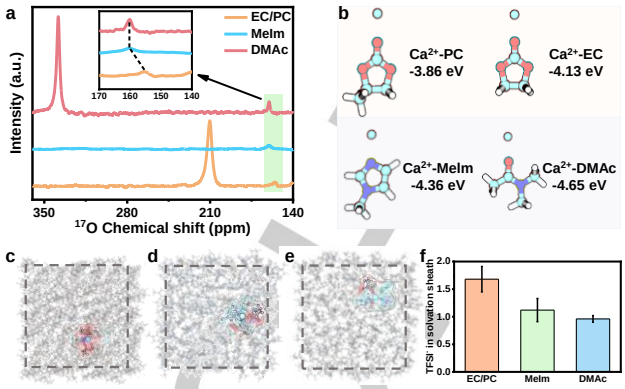

Figure 2. Revealing the solvation structures. a) ^{17}O NMR spectra of 0.1 M $Ca(TFSI)_2$ in different solvents. b) Relaxed geometries of the Ca^{2+}-solvent complex. The binding energies are calculated using density functional theory. Snapshots of MD simulations of 0.5 M $Ca(TFSI)_2$ in c) EC/PC, d) MeIm and e) DMAc solvents. $TFSI^-$ anions are highlighted in the 1st solvation sheath of Ca^{2+}. f) Number of $TFSI^-$ in 1st solvation sheath of Ca^{2+} in 0.5 M $Ca(TFSI)_2$ electrolytes from MD simulations.

resistance (R_{int}) of ~4 × 10^3 kΩ. In contrast, MeIm and DMAc electrolytes result in lower values of ~700 kΩ (Figure S3 and Figure 1d), consistent with the reduced overpotentials in Ca|Ca cells. These observations imply that the Ca deposition/stripping process is deeply associated with interfacial characteristics.

The SEIs features are largely dictated by the electrolyte solvation structure,[12, 15] which is assessed through the Raman spectra and ^{17}O nuclear magnetic resonance (NMR) spectroscopy. The Ca^{2+}-$TFSI^-$ coordination structure is examined through the S-N-S binding frequency in $TFSI^-$.[16] EC/PC electrolyte displays two S-N-S bending vibration modes corresponding to free ion (FI, $TFSI^-$ without Ca^{2+} coordination) and loose ion pair (LIP, $TFSI^-$ coordinating with Ca^{2+}). In comparison, only FI is discovered in MeIm and DMAc electrolytes (Figure S4). It indicates the weakest capability of EC/PC in dissolving $Ca(TFSI)_2$ among these solvents. We further inspect their solvation ability using ^{17}O NMR. A chemical shift at ~155.3 ppm presented in EC/PC electrolyte is assigned to the sulfonyl oxygen of $TFSI^-$, while this peak increases to ~160.1 ppm in MeIm and DMAc electrolytes (Figure 2a and Figure S5). This observation suggests the weaker ion-dipole interactions between $TFSI^-$ and Ca^{2+} in MeIm and DMAc electrolytes compared with EC/PC case, which agrees with the Raman results.

DN is a powerful indicator for the initial screening of the potential solvent because of its critical effect on determining the solvation structure.[17] Since the solvation structure could be also affected by other parameters, we perform quantum chemical computations and large-scale molecular dynamics (MD) simulations based on machine learning force fields, to further probe the atomistic details of solvation structures and correlate them with macroscopic Ca deposition stability. As shown in Figure 2b, binding energies between Ca^{2+} with PC, EC, MeIm and DMAc are -3.86, -4.13, -4.36 and -4.65 eV, respectively. Such a result indicates a high affinity of MeIm and DMAc with Ca^{2+}. This agrees with our experimental observation that MeIm and DMAc solvents possess strong solvating power than EC/PC. Benefiting from the high solvating ability, solvent-dominated solvation structures are expected to form in MeIm and DMAc electrolytes. It is validated by simulating bulk electrolytes using

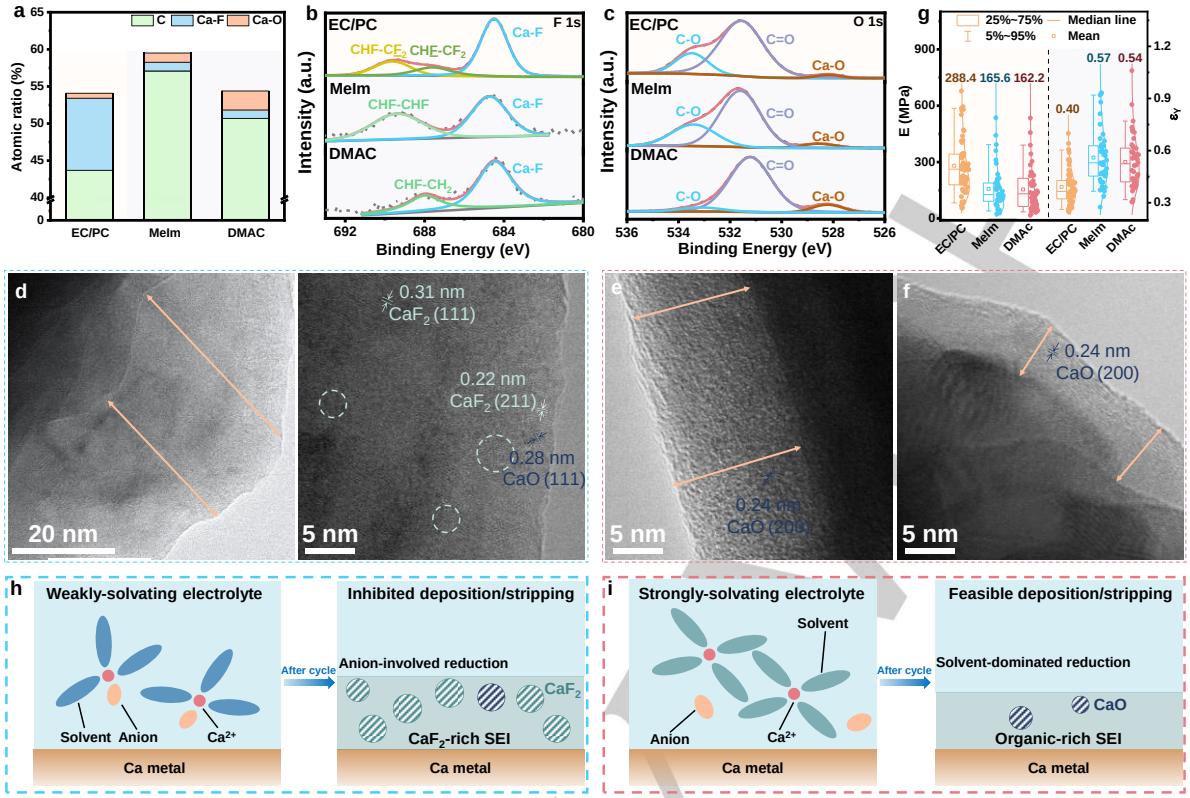

Figure 3. Probing the SEIs structures. a) The atomic ratio of C element, CaF_2 and CaO species in the SEIs. XPS spectra of b) F 1s and c) O 1s. TEM characterization of the SEIs formed in d) EC/PC, e) MeIm and f) DMAc electrolytes. g) Mechanical properties of the SEIs. Illustrations of the solvation structure and SEIs feature in h) weakly- and i) strongly-solvating electrolytes.

large-scale MD simulations. As shown in the snapshots in Figure 2c-e, the first solvation sheath of Ca^{2+} in EC/PC electrolyte shows a much stronger $TFSI^-$-rich characteristic than that of MeIm and DMAc cases regardless of the concentration (The statistics are detailed in Figure 2f and Figure S6). These systematic results confirm the formation of solvent-dominated solvation sheaths in strongly-solvating MeIm and DMAc electrolytes, which may constitute the major reasons for the enhanced Ca deposition/stripping behavior.

Having determined the solvent-dominated solvation sheaths conducing to reversible Ca deposition/stripping, we then aim to disclose their effects on SEIs properties. X-ray photoelectron spectroscopy (XPS) is collected to analyze the chemical compositions of SEIs in these electrolytes. The SEIs in the three electrolytes have similar compositions, which consist of organic and inorganic species, as revealed by the deconvoluted C 1s, O 1s and F 1s spectra (Figure S7). Nevertheless, they differ significantly in the relative amounts of each component. The SEIs formed in MeIm and DMAc electrolytes have a high carbon content of over 50.0%, while the one in EC/PC counterpart possesses only 43.7% carbon (Figure 3a). It illustrates the formation of organic-rich SEIs under strongly-solvating electrolytes that are predominantly derived from solvent reduction. Detailed analysis of the F and O peaks suggests CaF_2 and CaO are the major inorganic phases (Figure 3b and c). A large amount of CaF_2 (9.6%) is presented in the EC/PC-derived SEIs, resulting from the excessive anion ($TFSI^-$) decomposition. Noteworthy, it is widely recognized that CaF_2 inhibits Ca deposition/stripping,[8b, 9] explaining the poor reversibility in EC/PC electrolytes. In comparison, the SEIs in strongly-solvating electrolytes (MeIm and DMAc) show merely ~1.0% CaF_2 due to the minor $TFSI^-$ participated in the solvation structures. These observations agree with the cyclic voltammetry (CV) results where the anion reduction process is suppressed in strongly-solvating electrolytes (Figure S8)

The observation is further confirmed by transmission electron microscopy (TEM). The SEIs are grown on Cu particles for clear visualization (Detailed preparation process is provided in the experimental section). A thick SEI of around 30 nm is found under EC/PC electrolyte (Figure 3d), compared to about 13 and 6 nm for those in MeIm and DMAc electrolytes (Figure 3e and f), respectively. The thick SEIs elongate the Ca^{2+} diffusion pathways and potentially impairs the kinetics. Moreover, abundant CaF_2 nanoparticles are observed in the EC/PC-derived SEIs, whereas the SEIs in MeIm and DMAc electrolytes consist of an amorphous polymer matrix with minor CaO particles embedded. Such a composition difference could also be reflected in the mechanical properties of the SEIs. Such a composition difference could also be reflected in the mechanical properties of the SEIs owing to lower Young's modulus (E) and higher elastic strain limit (ε_Y) of organic components than inorganic ones. Because of the high content of inorganic species, the SEIs in EC/PC electrolyte shows a larger E and lower ε_Y, as examined by atomic force microscopy (AFM)-based nanoindentation tests (Figure 3g). Based on these results, we depict the relation between electrolyte recipes/solvation sheaths and SEIs structures in Figure 3h and i. Specifically, inorganic-rich SEIs derived mainly from anion reduction is formed in the

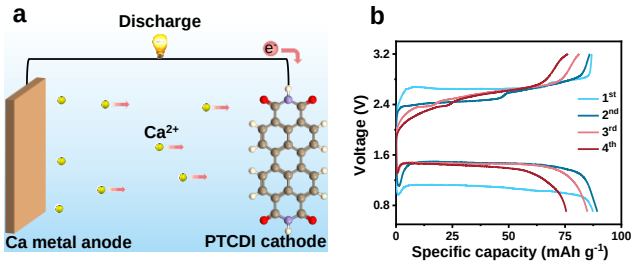

Figure 4. Full cell demonstration. a) Work schematic of the full cell using Ca metal anode and PTCDI cathode during the discharge process. b) Voltage profiles of the cell in DMAc electrolyte at 50 mA g^{-1}.

weakly-solvating electrolyte, which inhibits Ca deposition/stripping. In contrast, the solvent-dominated solvent sheath in strongly-solvating electrolytes contributes to an organic-rich SEI, enabling a feasible Ca metal anode (The potential ion-conducting mechanism has been discussed in Figure S9 and S10).

Last, we assess the potential application of the optimized electrolytes by pairing the Ca metal anodes with a new 3,4,9,10-perylenetetracarboxylic diimide (PTCDI) organic cathode (Figure 4a). The cell could be reversibly discharged/charged in both DMAc and MeIm electrolytes (Figure 4b and Figure S11). The calciation behavior in PTCDI cathode is probed by EDS elemental mapping (Figure S12). Although the cell shows a capacity fading arising from the PTCDI dissolution in the electrolyte (Figure S13), it proves the feasibility of these electrolytes in enabling reversible Ca metal anodes.

We now discuss the discrepancy of interface design between Ca and Li metal anodes because we note the solvents adopted here are incompatible with the LIBs' anodes and rarely used,[18] where carbonate solvents are most preferred. To explore the underlying reasons, we compare the SEIs constructed in Li metal anode under classic EC/PC- and the DMAc- based electrolytes with LiTFSI as the salt. The XPS analysis confirms the high solvation capability of DMAc promotes the formation of organic components in SEIs (Figure S14). Nevertheless, the Li deposition/stripping shows a stark contrast to Ca metal counterparts (Figure S15a). It delivers much smaller over-potential and longer cyclic life in EC/PC electrolytes. A similar phenomenon exists in Na and K metal anodes, where DMAc solvent obstructs the reversible cycling (Figure S15b and c). Further exploiting this direction, we extend our study to Mg metal anodes, which are afflicted by the similar passivating SEIs with Ca. Encouragingly, DMAc solvent benefits the reversible Mg deposition/stripping compared to EC/PC counterpart (Figure S16). The SEIs characteristics also follow the trend discussed before, i.e., the DMAc favors the formation of SEIs with an increased amount of organic components (Figure S17). This phenomenon seems to be reconciled in all the systems regardless of the cation type because of the formation of solvent-dominant solvation structure in DMAc electrolytes, but their effects differ significantly on alkali-metal (Li, Na, K) and alkaline-earth metal (Mg, Ca) anodes.

The above observations do not come as a surprise, considering the distinct ionic conductivity of the inorganic components in their SEIs, which is reflected by the EIS results (Figure S18). Ca metal anodes present high R_{int} of over 700 kΩ, while Li counterparts show three orders of magnitude lower values (~500 Ω). In general, inorganic species, such as LiF and Li_2CO_3, advance the Li^+ charge transfer.[19] An inorganic-rich SEI is desired in many reported Li-systems. Turning to the divalent batteries, the detrimental inorganic species, like CaF_2 and $CaCO_3$, should be minimized. Such a requirement reflects on not only the solvent selection but also the electrolyte concentration. An increase in the concentration of $Ca(TFSI)_2$/DMAc and $Ca(TFSI)_2$/MeIm electrolyte essentially degrades the performance (Figure S20a). It explains why a low salt concentration, normally no greater than 0.5 M, is adopted in Mg and Ca batteries,[8a] as the increased concentration urges the anion reduction for producing inorganic components.[10a] Apart from the solvent and concentration, the solvation structure could also be tuned by the salt. We examine the DMAc electrolytes with $Ca(CF_3SO_3)_2$ and $Ca(FSI)_2$ salts. They present worse performance than $Ca(TFSI)_2$ salt due to the strong coordination between the cation and anion in the former two salts (Figure S20b), making them more challenging to be dissociated to allow sufficient solvent participation in the cation solvation sheath.

In summary, we reveal that a solvent-dominated solvation sheath of cation is preferred in the emerging Ca system, which could be realized through solvent, salt and concentration optimization. This leads to the design of several promising electrolyte formulations for the reversible Ca plating/stripping under a commercially available salt $Ca(TFSI)_2$ at room temperature for the first time. Although slightly large deposition/stripping overpotentials are still observed, this may be solved in the future by fabricating a Ca^{2+}-conducting artificial interface on Ca metal to complement the SEIs to boost Ca^{2+} transfer. Furthermore, a systematic comparison of the interface chemistry between Ca metal anodes and Li/Na/K systems shows the paradigm shift in SEIs design for emerging RCMBs, providing a guide to electrolyte formulation development.

Acknowledgements

This work was supported by the General Research Fund (GRF) scheme of the Hong Kong Research Grants Council (Project No. 15306422) and the Hong Kong Polytechnic University (ZE2F). We gratefully acknowledge the support of the University Research Facility on Chemical and Environmental Analysis (UCEA) of PolyU. Z.H. is grateful to Dr. Y. Gao and Ms. D. Wang for assistance in AFM test. Y.Z. acknowledges the financial support from the Research Grants Council of Hong Kong (Project No. C5029-18E). Z.L. thanks the Bin Shao and Tie-Yan Liu from Microsoft Research for the help in computational resources.

Keywords: Ca deposition/stripping • electrolyte formulation • solvation structure • solid electrolyte interphase

[1] a) M. Armand, J. M. Tarascon, *Nature* **2008**, *451*, 652-657; b) R. J. Gummow, G. Vamvounis, M. B. Kannan, Y. He, *Adv. Mater.* **2018**, *30*, e1801702; c) B. Ji, H. He, W. Yao, Y. Tang, *Adv. Mater.* **2021**, *33*, e2005501; d) Z. Liang, C. Ban, *Angew. Chem. Int. Ed. Engl.* **2021**, *60*, 11036-11047; e) Y. Liang, H. Dong, D. Aurbach, Y. Yao, *Nature Energy* **2020**, *5*, 646-656; f) X. Li, T. Gao, F. Han, Z. Ma, X. Fan, S. Hou, N. Eidson, W. Li, C. Wang, *Advanced Energy Materials* **2017**, *8*.

[2] a) I. D. Hosein, *ACS Energy Letters* **2021**, *6*, 1560-1565; b) M. E. Arroyo-de Dompablo, A. Ponrouch, P. Johansson, M. R. Palacin, *Chem. Rev.* **2020**, *120*, 6331-6357; c) K. V. Nielson, T. L. Liu, *Angew. Chem. Int. Ed. Engl.* **2020**, *59*, 3368-3370; d) M. Wang, C. Jiang, S. Zhang, X. Song, Y. Tang, H. M. Cheng, *Nat Chem* **2018**, *10*, 667-672.

[3] a) R. J. Staniewicz, *J. Electrochem. Soc.* **1980**, *127*, 782; b) D. Aurbach, R. Skaletsky, Y. Gofer, *J. Electrochem. Soc.* **1991**, *138*, 3536-3545; c) L. Stievano, I. de Meatza, J. Bitenc, C. Cavallo, S. Brutti, M. A. Navarra, *J. Power Sources* **2021**, *482*; d) A. M. Melemed, B. M. Gallant, *J. Electrochem. Soc.* **2020**, *167*.

[4] a) S. Biria, S. Pathreeker, H. Li, I. D. Hosein, *ACS Applied Energy Materials* **2019**, *2*, 7738-7743; b) X. Gao, X. Liu, A. Mariani, G. A. Elia, M. Lechner, C. Streb, S. Passerini, *Energy & Environmental Science* **2020**, *13*, 2559-2569; c) S. Hou, X. Ji, K. Gaskell, P. F. Wang, L. Wang, J. Xu, R. Sun, O. Borodin, C. Wang, *Science* **2021**, *374*, 172-178; d) N. T. Hahn, J. Self, D. M. Driscoll, N. Dandu, K. S. Han, V. Murugesan, K. T. Mueller, L. A. Curtiss, M. Balasubramanian, K. A. Persson, K. R. Zavadil, *Phys. Chem. Chem. Phys.* **2022**, *24*, 674-686; e) K. Kisu, S. Kim, T. Shinohara, K. Zhao, A. Zuttel, S. I. Orimo, *Sci Rep* **2021**, *11*, 7563; f) Y. Jie, Y. Tan, L. Li, Y. Han, S. Xu, Z. Zhao, R. Cao, X. Ren, F. Huang, Z. Lei, G. Tao, G. Zhang, S. Jiao, *Angew. Chem. Int. Ed. Engl.* **2020**, *59*, 12689-12693.

[5] A. Ponrouch, C. Frontera, F. Barde, M. R. Palacin, *Nat Mater* **2016**, *15*, 169-172.

[6] R. Mohtadi, M. Matsui, T. S. Arthur, S. J. Hwang, *Angewandte Chemie* **2012**, *124*, 9918-9921.

[7] D. Wang, X. Gao, Y. Chen, L. Jin, C. Kuss, P. G. Bruce, *Nat Mater* **2018**, *17*, 16-20.

[8] a) Z. Li, O. Fuhr, M. Fichtner, Z. Zhao-Karger, *Energy & Environmental Science* **2019**, *12*, 3496-3501; b) A. Shyamsunder, L. E. Blanc, A. Assoud, L. F. Nazar, *ACS Energy Letters* **2019**, *4*, 2271-2276.

[9] J. Forero-Saboya, C. Davoisne, R. Dedryvère, I. Yousef, P. Canepa, A. Ponrouch, *Energy & Environmental Science* **2020**, *13*, 3423-3431.

[10] a) G. M. Hobold, J. Lopez, R. Guo, N. Minafra, A. Banerjee, Y. Shirley Meng, Y. Shao-Horn, B. M. Gallant, *Nature Energy* **2021**, *6*, 951-960; b) J. Liu, Z. Bao, Y. Cui, E. J. Dufek, J. B. Goodenough, P. Khalifah, Q. Li, B. Y. Liaw, P. Liu, A. Manthiram, Y. S. Meng, V. R. Subramanian, M. F. Toney, V. V. Viswanathan, M. S. Whittingham, J. Xiao, W. Xu, J. Yang, X.-Q. Yang, J.-G. Zhang, *Nature Energy* **2019**, *4*, 180-186.

[11] H. Song, J. Su, C. Wang, *Advanced Energy Materials* **2021**, *11*, 2003685.

[12] C. Yan, H. R. Li, X. Chen, X. Q. Zhang, X. B. Cheng, R. Xu, J. Q. Huang, Q. Zhang, *J. Am. Chem. Soc.* **2019**, *141*, 9422-9429.

[13] Y. Jie, X. Liu, Z. Lei, S. Wang, Y. Chen, F. Huang, R. Cao, G. Zhang, S. Jiao, *Angew. Chem. Int. Ed. Engl.* **2020**, *59*, 3505-3510.

[14] L. Johnson, C. Li, Z. Liu, Y. Chen, S. A. Freunberger, P. C. Ashok, B. B. Praveen, K. Dholakia, J. M. Tarascon, P. G. Bruce, *Nat Chem* **2014**, *6*, 1091-1099.

[15] a) H. Cheng, Q. Sun, L. Li, Y. Zou, Y. Wang, T. Cai, F. Zhao, G. Liu, Z. Ma, W. Wahyudi, Q. Li, J. Ming, *ACS Energy Letters* **2022**, *7*, 490-513; b) D. M. Driscoll, N. K. Dandu, N. T. Hahn, T. J. Seguin, K. A. Persson, K. R. Zavadil, L. A. Curtiss, M. Balasubramanian, *J. Electrochem. Soc.* **2020**, *167*; c) J. D. Forero-Saboya, E. Marchante, R. B. Araujo, D. Monti, P. Johansson, A. Ponrouch, *J Phys Chem C Nanomater Interfaces* **2019**, *123*, 29524-29532; d) N. T. Hahn, D. M. Driscoll, Z. Yu, G. E. Sterbinsky, L. Cheng, M. Balasubramanian, K. R. Zavadil, *ACS Applied Energy Materials* **2020**, *3*, 8437-8447.

[16] L. Suo, F. Zheng, Y.-S. Hu, L. Chen, *Chinese Physics B* **2016**, *25*.

[17] Z. Wang, Z. Sun, J. Li, Y. Shi, C. Sun, B. An, H.-M. Cheng, F. Li, *Chem. Soc. Rev.* **2021**, *50*, 3178-3210.

[18] A. Gupta, A. Bhargav, A. Manthiram, *Advanced energy materials* **2019**, *9*, 1803096.

[19] Z. Yu, P. E. Rudnicki, Z. Zhang, Z. Huang, H. Celik, S. T. Oyakhire, Y. Chen, X. Kong, S. C. Kim, X. Xiao, *Nature Energy* **2022**, *7*, 94-106.